COMPUTER METHODS IN BIOMECHANICS AND BIOMEDICAL ENGINEERING
2021, VOL. 24, NO. 3, 289–298
https://doi.org/10.1080/10255842.2020.1827236

Electroosmotically driven flow of micropolar bingham viscoplastic fluid in a wavy microchannel: application of computational biology stomach anatomy

Anber Saleem[a,b], Mishal Nayab Kiani[c], Sohail Nadeem[c], Salman Akhtar[c], Mehdi Ghalambaz[d,e] and Alibek Issakhov[f]

[a]Mathematics and its Applications in Life Sciences Research Group, Ton Duc Thang University, Ho Chi Minh City, Vietnam; [b]Faculty of Mathematics and Statistics, Ton Duc Thang University, Ho Chi Minh City, Vietnam; [c]Department of Mathematics, Quaid-i-Azam University 45320, Islamabad, Pakistan; [d]Institute of Research and Development, Duy Tan University, Da Nang, Vietnam; [e]Faculty of Electrical – Electronic Engineering, Duy Tan University, Da Nang, Vietnam; [f]Faculty of mechanics and mathematics, Al-Farabi Kazakh National University, Almaty, Kazakhstan

ABSTRACT

A comprehensive mathematical model is presented to study the peristaltic flow of Bingham viscoplastic micropolar fluid flow inside a microlength channel with electro-osmotic effects. The electro-osmotic effects are produced due to an axially applied electric field. The circulation of this electric potential is calculated by utilizing Poisson Boltzmann equation. The dimensionless form of mathematical equations is obtained by using lubrication theory and Debye-Huckel approximation. We have obtained analytical solutions for the final dimensionless governing equations. Finally, the graphical results are added to further discuss the physical aspects of the problem. Electro-osmotic is mainly helping to control the flow and axial velocity decreases with an increase in the electric field but micro-angular velocity increases with an increase in electric field.

ARTICLE HISTORY
Received 4 August 2020
Accepted 19 September 2020

KEYWORDS
Electroosmosis; Peristalsis; Micropolar fluid; Non-Newtonian flow; wall shear stress

1. Introduction

The peristaltic flow phenomenon has a key role in many physiological flow problems that are related to human body. Latham (Latham 1966) had interpreted mathematically the physiological flow inside human body that involves peristalsis mechanism. These physiological flow problems involve the stomach anatomy (i.e., movement of food bolus inside digestive tract) and transport of urine from kidneys to bladder. Both these physiological flow problems include peristalsis mechanism.

The analytical solutions are obtained for peristaltic flow in a vertical channel by Abumandour et al (2020). Abdelsalam (Abdelsalam and Mekheimer 2018) had presented a model to obtain the closed form analytical solutions for peristaltic flow problem. Bhatti (Abdelsalam and Bhatti, 2018a) had mathematically interpreted the peristaltic flow with hall and slip effects. The peristaltic flow of Prandtl fluid with nanoparticles was examined by Abdelsalam and Bhatti (2018b). Vafai (Abdelsalam and Vafai, 2017a) had presented the mathematical study of electro-osmotically driven flow inside microfluidic channels. The numerical, analytical and experimental research problems related to peristaltic flow phenomenon for distinct fluid models is presented under different conditions with reference to diverse mechanical and physiological applications (Shapiro et al. 1969; Jaffrin and Shapiro 1971; Srivastava and Srivastava 1984; Mekheimer and Abd Elmaboud 2008; Pandey and Tripathi 2011). Peristaltic pumps have many uses in transporting blood, slurry, food and corrosive liquids etc. Some recent studies that include the analysis of flow in microfluidic channels and their applications is provided (Elkoumy et al. 2013; Mekheimer et al. 2013; Abdelsalam and Vafai, 2017b; Abd Elmaboud et al. 2019; Abdelsalam et al. 2019; Abdelsalam and Bhatti 2019; Eldesoky, Abdelsalam, El-Askary, Ahmed 2019; Eldesoky, Abdelsalam, El-Askary, El-Refaey, et al. 2019).

The pumping mechanism that is used to transport the fluid inside a microfluidic device has significant importance due to its applications. The electro-osmotic flow phenomenon has advantage over magnetohydrodynamics, piezoelectrics and electrohydrodynamics due to its simple design, comparatively low cost and their relaxed fabrication (van Lintel et al. 1988; Richter et al. 1991; Arulanandam and Li 2000; Lemoff and Lee 2000).

CONTACT S. Nadeem sohail@qau.edu.pk

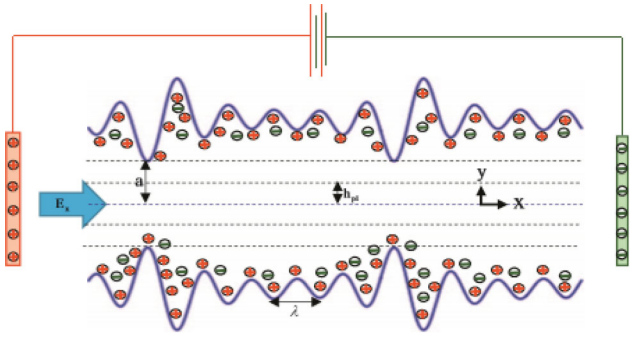

Figure 1. Flow geometry for wavy channel.

The flow is fully developed without the movement of any mechanical part. The basic peristalsis principle and electro-osmotic effects are used in working of many micro-pumps. The highly applicable areas of electro-osmosis phenomenon involve drug delivery by diagnostic medical apprautus, treatment of diseases, (i.e., sickle cell, anomaly in cells and blood related medical problems.). Some important non-Newtonian fluid models are given (Khan et al. 2018; Qayyum et al. 2018; Khan et al. 2019).

Further, main advantages of such electro-osmotic pumps are their efficiency and low cost working. The pumps that include combine benefits of both electro-osmosis and peristalsis are widely used due to their applications. Some recent studies that provide useful results are also provided (Hayat et al. 2016; Khan et al. 2017; Abbas, Khan, Kadry, Khan, Waqas, et al. 2020; Abbas, Khan, Kadry, Khan, Israr-Ur-Rehman, et al., 2020; Khan et al., 2020a; 2020b; Nayak et al. 2020; Wang, Muhammad, et al. 2020).

Flow activities of non-Newtonian fluids have larger prominence as they occur extensively in several physiological fluids and other fluids used in various productions. The non-Newtonian fluid flow problems have been extensively explored (Misra et al. 2001; Misra and Ghosh 2001; Dhinakaran et al. 2010; Maiti and Misra 2012). Various non-Newtonian models of fluid exist in the literature (Haghighi et al. 2015; Haghighi and Asl 2015; Abdelsalam and Bhatti 2020; Abdelsalam and Sohail 2020; Haghighi et al. 2020; Sadaf and Abdelsalam 2020; Sohail et al. 2020) and for combined electroosmotic flow including slit microchannel for Casson fluid (Ng and Qi 2014), Jeffrey fluid in corrugated microchannels (Si and Jian 2015), power-law fluids in non-uniform microchannels (Ng 2013), micropolar fluids in microchannels (Ding et al. 2016), Maxwell fluids in rectangular microchannels (Jiménez et al. 2016), Bingham model in wavy microchannels (Tripathi et al. 2018), and Nanofluidics channel (Ding et al. 2017). Some recent literature articles are provided (Ijaz Khan and Alzahrani 2020; Khan, Qayyum, et al., 2020; Muhammad et al. 2020; Wang, Khan, et al. 2020).

A complete descriptive literature analysis has depicted that the flow of Micropolar Bingham Viscoplastic fluid across a channel with wavy walls is not interpreted mathematically with electro-osmotic effects by anyone mathematically. The present analysis first time addresses this important topic of Micropolar Bingham viscoplastic fluid with the electroosmotic effects. Mainly, we have examined the peristaltic flow with combine electroosmosis effects and the micro-rotations that occur during this flow are also considered in this mathematical analysis. Electric field is employed in an axial direction. For fluid flow, a complex wavy microchannel is taken into account. Analytical solutions for axial and micro-angular velocity are obtained by using different methods of integration. Graphs for the closed-form solution are sketched for different parameters using mathematics software.

2. Mathematical configuration

2.1. Geometric structure

The flow geometry for Micropolar Bingham viscoplastic liquid in a microchannel influenced by electroosmosis is given in Figure 1. The geometry of deformable wall is presented by the following mathematical statement:

$$\overline{h}(\overline{x},\overline{t}) = a + \sum_{i=1}^{n} \overline{\phi}\sin\frac{2i\pi}{\lambda}(\overline{x} - c\overline{t}), \tag{1}$$

The value of n represents multiple sinusoidal waves. We have used n = 2 for our present study. here $\overline{h}$ characterizes transverse ocilliation of the channle's wall, a indicate the half-width of the microchannel, $\overline{\phi}$ symbolizes the waves amplitude, λ and c designates wavelength and wave speed, $\overline{x}$ and $\overline{t}$ signifies, axial coordinate, and time, respectively.

2.2. Fluid model

Mathematical expression for Micropolar Bingham viscoplastic fluids is given as (Shelukhin and Neverov 2016):

$$\begin{aligned} \overline{\tau} &= \overline{\tau}_0 + (\mu + k)\dot{\gamma} + kN, \ \ \overline{\tau} \geq \overline{\tau}_0 \\ \dot{\gamma} &= 0, \ \ \overline{\tau} < \overline{\tau}_0 \end{aligned} \tag{2}$$

here $\overline{\tau}$ and $\overline{\tau}_0$ reveal the shear and the yield stress, μ is the viscosity of the fluid, $\dot{\gamma}$ indicates the shear

strain rate, and k represents the vortex viscosity of the fluid.

2.3. Governing equations

The mathematical equations govenring the flow of a Micropolar Bingham viscoplastic fluid subject to an electric field are provided by (Pandey and Chaube 2011):

$$\frac{\partial \overline{u}}{\partial \overline{x}} + \frac{\partial \overline{v}}{\partial \overline{y}} = 0, \tag{3}$$

$$\rho\left(\frac{\partial \overline{u}}{\partial \overline{t}} + \overline{u}\frac{\partial \overline{u}}{\partial \overline{x}} + \overline{v}\frac{\partial \overline{u}}{\partial \overline{y}}\right) + \frac{\partial \overline{p}}{\partial \overline{x}} - \frac{\partial \overline{\tau}_{\overline{x}\overline{x}}}{\partial \overline{x}} - \frac{\partial -\overline{\tau}_{\overline{x}\overline{y}}}{\partial \overline{y}} - \rho_e E_x = 0, \tag{4}$$

$$\rho\left(\frac{\partial \overline{v}}{\partial \overline{t}} + \overline{u}\frac{\partial \overline{v}}{\partial \overline{x}} + \overline{v}\frac{\partial \overline{v}}{\partial \overline{y}}\right) + \frac{\partial \overline{p}}{\partial \overline{y}} - \frac{\partial -\overline{\tau}_{\overline{y}\overline{x}}}{\partial \overline{x}} - \frac{\partial -\overline{\tau}_{\overline{y}\overline{y}}}{\partial \overline{y}} - \rho_e E_y = 0, \tag{5}$$

$$\rho\bar{j}\left(\frac{\partial \overline{N}}{\partial \overline{t}} + \overline{u}\frac{\partial \overline{N}}{\partial \overline{x}} + \overline{v}\frac{\partial \overline{N}}{\partial \overline{y}}\right) + 2k\overline{N} - \gamma\left(\frac{\partial^2 \overline{N}}{\partial \overline{x}^2} + \frac{\partial^2 \overline{N}}{\partial \overline{y}^2}\right) - k\left(\frac{\partial \overline{v}}{\partial \overline{x}} - \frac{\partial \overline{u}}{\partial \overline{y}}\right) = 0, \tag{6}$$

with the boundary conditions:

$$\overline{\tau}|_{\overline{y}=0} = 0,\ \overline{\tau}|_{\overline{y}=h_{pl}} = \overline{\tau}_0,\ \overline{u}|_{\overline{y}=\overline{h}} = 0,\ \left.\frac{\partial \overline{N}}{\partial \overline{y}}\right|_{\overline{y}=0} = 0,\ \overline{N}|_{\overline{y}=\overline{h}} = 0, \tag{7}$$

where ρ is fluid's density, $\overline{u}$ and $\overline{v}$ are the velocities in an axial and transverse direction, $\overline{p}$ is pressure, $\overline{\tau}_{\overline{x}\overline{x}}$, $\overline{\tau}_{\overline{x}\overline{y}}$, $\overline{\tau}_{\overline{y}\overline{x}}$, $\overline{\tau}_{\overline{y}\overline{y}}$ are the components of stress, E_x and E_y are components of the electric field $\overline{E}$, $\overline{N}$ is micro-angular velocity, $\bar{j}$ signifies the micro-inertia per unit mass, γ defines the spin gradient velocity and ρ_e is the total ionic charge's density.

Presenting the dimensionless parameters to get closed-form solutions of modeled flow equations,

$$\begin{aligned} &x = \frac{\overline{x}}{\lambda},\ y = \frac{\overline{y}}{a},\ t = \frac{\overline{t}c}{\lambda},\ u = \frac{\overline{u}}{c},\ v = \frac{\overline{v}}{\delta c},\ h = \frac{\overline{h}}{a},\\ &\phi = \frac{\overline{\phi}}{a},\ \delta = \frac{a}{\lambda},\\ &\tau = \frac{\overline{\tau}a}{\mu c},\ \tau_0 = \frac{\tau_0 a}{\mu c},\ p = \frac{\overline{p}a^2}{\mu c\lambda},\ \varphi = \frac{ze\overline{\varphi}}{k_B T},\\ &n = \frac{\overline{n}}{n_0},\quad N = \frac{a}{c}\overline{N},\ j = \frac{\bar{j}}{a^2}. \end{aligned} \tag{8}$$

where τ_0 and τ are the non-dimensional yield and shear stress, ϕ is the non-dimensional amplitude of waves, δ stands for the peristaltic wave number, and φ denotes the non-dimensional electric potential.

The contact between aqueous electrolytic solution and the solid surface generally results in electrostatic charge on the surface that is known as zeta potential. Electric double-layer (EDL) appears when the charged surface fascinates the counter ions toward itself in the solution. Due to zeta potential, the electrical potential in the solution follows the Poisson equation stated as:

$$\nabla^2 \overline{\varphi} = -\frac{\rho_e}{\varepsilon}, \tag{9a}$$

where $\overline{\varphi}$ designates the electrical potential, ∇^2 symbolizes the two-dimensional Laplace operator, and ρ_e is the density of total ionic charge, and ε is the electrical permittivity of ionic solution.

Potential function φ can be obtained as given in (Nadeem et al. 2020).

$$\varphi = \frac{\cosh(\kappa y)}{\cosh(\kappa h)}. \tag{9b}$$

Invoking dimensionless parameters and lubrication approcimation is used, (i.e., large wavelength and low Reynolds number assumptions), Eqs. (1–6), take the form:

$$h(x,t) = 1 + \sum_{i=1}^{n} \phi \sin 2\pi(x-t), \tag{10}$$

$$\begin{aligned} \tau &= \tau_0 + \left(\frac{\mu + k}{\mu}\right)\frac{\partial u}{\partial y} + \frac{k}{\mu}N,\ \ \tau \geq \tau_0\\ \frac{\partial u}{\partial y} &= 0,\ \ \tau < \tau_0 \end{aligned} \tag{11}$$

$$\frac{\partial u}{\partial x} + \frac{\partial v}{\partial y} = 0, \tag{12}$$

$$\frac{\partial \tau_{xy}}{\partial y} = \frac{\partial p}{\partial x} - \kappa^2 u_e \frac{\cosh(\kappa y)}{\cosh(\kappa h)}, \tag{13}$$

$$\frac{\partial p}{\partial y} = 0, \tag{14}$$

$$\left(\frac{2-w}{m^2}\right)\frac{\partial^2 N}{\partial y^2} - 2\mathrm{N} - \frac{\partial u}{\partial y} = 0, \tag{15}$$

where $u_e = -\frac{E_x \varepsilon \zeta}{\mu c}$ is Helmholtz-Smoluchowski velocity, $w = \frac{k}{\mu + k}$ denotes coupling number and $m^2 = \frac{a^2 k(2\mu + k)}{\gamma(\mu + k)}$ is micropolar parameter.

3. Analytical solution

Substituting Eq. (11) in Eq. (13), we obtain,

$$\frac{\partial^2 u}{\partial y^2} + w\frac{\partial N}{\partial y} + (1-w)\left(-\frac{\partial p}{\partial x} + \kappa^2 u_e \frac{\cosh(\kappa y)}{\cosh(\kappa h)}\right) = 0, \tag{16}$$

with the dimensionless boundary conditions,

$$\left.\frac{\partial u}{\partial y}\right|_{y=h_{pl}} = -wN,\quad u|_{y=h}=0,\quad \left.\frac{\partial N}{\partial y}\right|_{y=0}=0,\quad N|_{y=h}=0. \tag{17}$$

Solving Eq. (15) and Eq. (16) using Eq. (17) we attain the solution of the form,

$$N = B\cosh(my) + C\sinh(my) - \frac{(1-w)}{(2-w)}\left(\frac{\partial p}{\partial x}y + \frac{\kappa m^2 u_e}{(\kappa^2-m^2)}\frac{\sinh(\kappa y)}{\cosh(\kappa h)}\right) - \frac{A}{(2-w)}. \tag{18}$$

$$u = -w\left(\frac{B}{m}\sinh(my) + \frac{C}{m}\cosh(my) - \frac{(1-w)}{(2-w)}\left(\frac{\partial p}{\partial x}\frac{y^2}{2} + \frac{m^2u_e}{\kappa^2-m^2}\frac{\cosh(\kappa y)}{\cosh(\kappa h)}\right) - \frac{Ay}{(2-w)}\right) + (1-w)\left(\frac{\partial p}{\partial x}\frac{y^2}{2} - u_e\frac{\cosh(\kappa y)}{\cosh(\kappa h)}\right) + Ay + D. \tag{19}$$

The expression for volumetric flow rate is signified as

$$Q = \int_{h_{pl}}^{h} u dy. \tag{20}$$

Using Eq. (19) in Eq. (20) and integrating, we obtain:

$$Q = -w\left(\frac{B}{m^2}\left(\cosh(mh)-\cosh(mh_{pl})\right) + \frac{C}{m^2}\left(\sinh(mh)-\sinh(mh_{pl})\right) - \frac{(1-w)}{(2-w)}\left(E + \frac{Fm^2u_e}{\kappa(\kappa^2-m^2)}\right) - \frac{A}{2(2-w)}\left(h^2-{h_{pl}}^2\right)\right) + (1-w)\left(\mathrm{E} - F\frac{u_e}{\kappa}\right) + \frac{A}{2}\left(h^2-{h_{pl}}^2\right) + D\left(h-h_{pl}\right). \tag{21}$$

where,

$$A = (1-w)\left(-\frac{\partial p}{\partial x}y + \kappa u_e\frac{\sinh(\kappa h_{pl})}{\cosh(\kappa h)}\right), \tag{22}$$

$$B = \frac{-1}{\cosh(mh)}\left(C\sinh(mh) - \frac{(1-w)}{(2-w)}\left(\frac{\partial p}{\partial x}h + \frac{\kappa m^2u_e}{\kappa^2-m^2}\tanh(\kappa h)\right) - \frac{A}{(2-w)}\right), \tag{23}$$

$$C = \frac{(1-w)}{(2-w)}\left(\frac{1}{m}\frac{\partial p}{\partial x} + \frac{\kappa^2 m u_e}{\kappa^2-m^2}\frac{1}{\cosh(\kappa h)}\right), \tag{24}$$

$$D = w\left(\frac{B}{m}\sinh(mh) + \frac{C}{m}\cosh(mh) - \frac{(1-w)}{(2-w)}\left(\frac{\partial p}{\partial x}\frac{h^2}{2} + \frac{m^2u_e}{\kappa^2-m^2}\right) - \frac{Ah}{(2-w)}\right) - (1-w)\left(\frac{\partial p}{\partial x}\frac{h^2}{2} - u_e\right) - Ah, \tag{25}$$

$$E = \frac{\partial p}{\partial x}\left(\frac{h^3}{6} - \frac{{h_{pl}}^3}{6}\right), \tag{26}$$

$$F = \left(\tanh(\kappa h) - \frac{\sinh(\kappa h_{pl})}{\cosh(\kappa h)}\right). \tag{27}$$

Pressure difference along unit wave length is given by:

$$\Delta p = \int_0^1 \frac{\partial p}{\partial x} dx. \tag{28}$$

The wave frame (x_w, y_w) and the laboratory frame (x, y) alterations are given by: $y = y_w,\ u = u_w + 1,\ x = x_w - t,\ v = v_w$, where (u, v) and (u_w, v_w) are the apparatuses of velocity in laboratory and wave frame respectively.

The volumetric flow rate is mathematically expressed by following expression

$$q_w = \int_{h_{pl}}^{h} u_w dy_w = \int_{h_{pl}}^{h} (u-1) dy_w, \tag{29}$$

after integration,

$$q_w = Q + 1 - h. \tag{30}$$

Flow rate along with a unit wave is specified as

$$\overline{Q} = \int_0^1 Q dt = \int_0^1 (q_w + h - h_{pl}) dt. \tag{31}$$

Explanation of the above equation yields,

$$\overline{Q} = (q_w + 1 - h_{pl}) = Q + 1 - h. \tag{32}$$

Shear stress at the wall can be calculated as:

$$\tau_{xy}|_{y=h} = \left(\tau_0 + \frac{1}{(1-w)}\frac{\partial u}{\partial y} + \frac{w}{(1-w)}N\right)\Big|_{y=h} \tag{33}$$

Substituting Eq. (25) and Eq. (26) in the above equation we obtain:

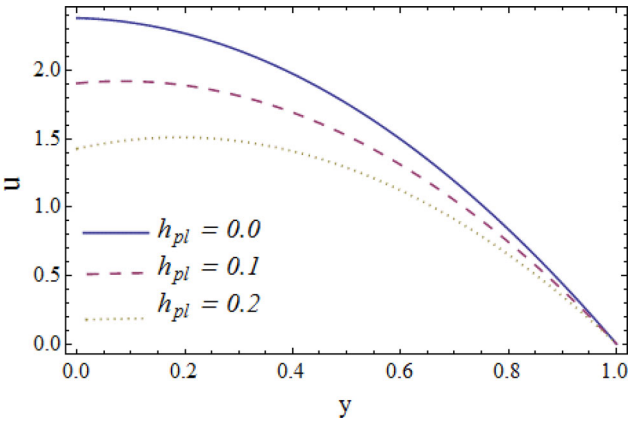

Figure 2. Impact of h_{pl} on velocity field with w = 0.2, m = 1, $\kappa = 2$, u_e, x = 1.

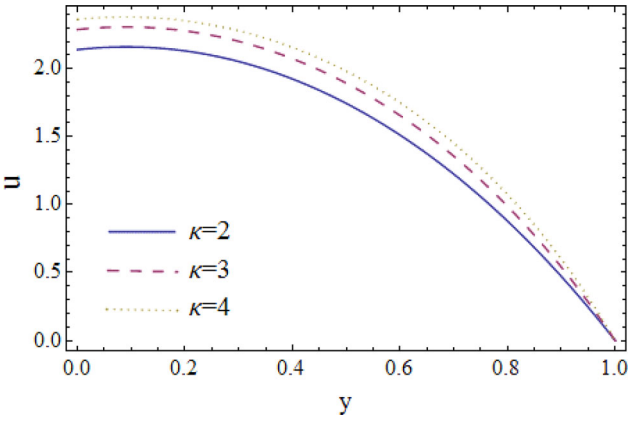

Figure 3. Impact of κ on velocity field with $x = 1$, u_e = 1, $h_{pl} = 0.1$, $m = 1$, $w = 0.2$.

$$\tau_{xy}|_{y=h} = \tau_0 + \frac{\partial p}{\partial x}h - \kappa u_e \tanh(\kappa h) + \frac{A}{(1-w)}. \quad (34)$$

4. Results and discussions

Figures 2–6 provides the variation of velocity u against $y - axis$ for changing values of Helmholtz-Smoluchowski velocity (u_e), Debye-length parameter (κ), plug flow width (h_{pl}) coupling number (w), and micropolar parameter (m^2). As illustrated in Figure 2, the velocity of fluid declines with the increasing values of plug flow. Figure 3 depicts that an increase in the value of κ also increases the axial flow.

In the case of Helmholtz-Smoluchowski velocity, $(u_e = -\frac{E_x \varepsilon \zeta}{\mu c})$, it is straight forward linked to the electric field in the axial direction E_x. Therefore, axial velocity increases with an increase in u_e as shown in Figure 4. Figure 5 shows the variation in velocity profile with an increase in the coupling number (w). As the coupling number is directly related to spin gradient velocity (k), so velocity profile decreases with the slight increase in w. Figure 6 depicts that the velocity profile increases slightly with the increase in the micropolar parameter.

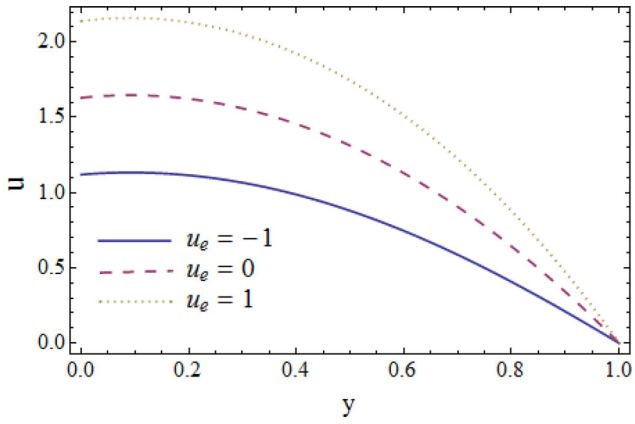

Figure 4. Impact of u_e on velocity field with $h_{pl} = 0.1$, x = 1, $\kappa = 2$, $m = 1$, $w = 0.2$.

Figures 7–11 represents the variation in micro-angular velocity. It is revealed from Eq.(7) that micro-angular velocity drops with increase in plug flow width (h_{pl}). However, with an increase in Helmholtz-Smoluchowski velocity (u_e) and the Debye-length parameter (κ), the micro-angular velocity profile increases as shown in Figures 8 and 9. Figure 10 depicts that the increase in coupling number (w) decreases the micro-angular velocity (N); however, for the micropolar parameter, N gains high value near the wall but declines far away from the wall as shown in Figure 11.

Figures 12–16 provides the relation between Δp and $\overline{Q}$, for different parameters. Evidently, Δp and $\overline{Q}$ are inversely related, which means that pressure difference decreases when the volumetric rate of the flow along unit time period increases. The increase in the value of plug flow width results in decline of ΔP, as displayed in Figure 12. A rise in the Debye-length parameter expressively increases the pressure difference, as shown in Figure 13. However, Δp reduces for 'negative' values of u_e, whereas, increases for 'positive' values of u_e as plotted in Figure 14. Figure 15 reveals that an increase in the coupling number reduces the pressure difference Δp along $\overline{Q}$, but an increase in micropolar parameter increases the pressure difference as plotted in Figure 16; however, an inverse linear relationship could be observed in all plots.

In Figures 17–19, we have plotted the shear stresses τ_{xy} at the wall $y = h$ for values of Helmholtz-Smoluchowski velocity (u_e), plug flow width (h_{pl}), and Debye-length parameter (κ) when the yield stress $\tau_0 = 2.3$. The wall shear stress decreases with the increase in all three parameters.

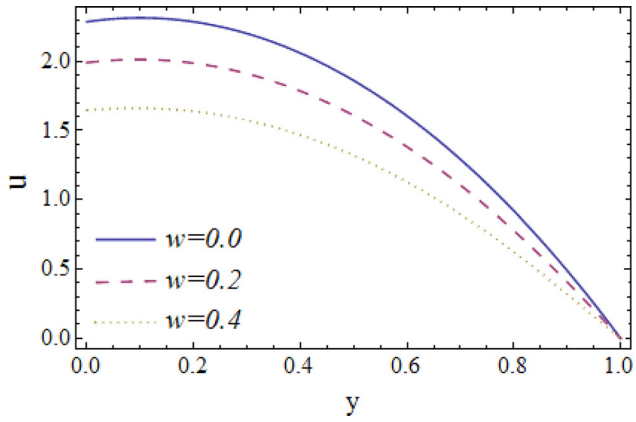

Figure 5. Impact of w on velocity field with $h_{pl} = 0.1$, $x = 1$, $\kappa = 2$, $m = 1$, $u_e = 1$.

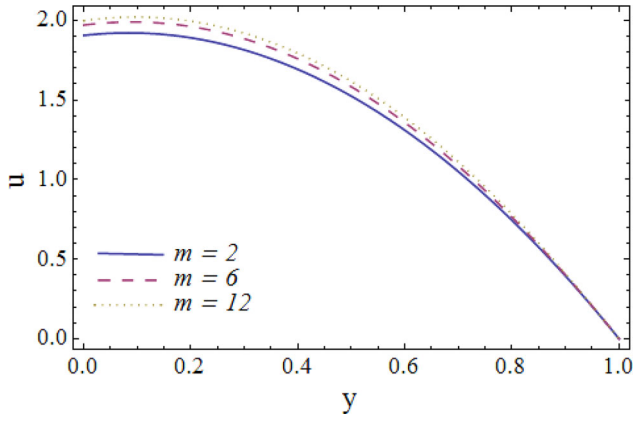

Figure 6. Impact of m on velocity field with $h_{pl} = 0.1$, $x = 1$, $\kappa = 1$, $w = 0.2$, $u_e = 1$.

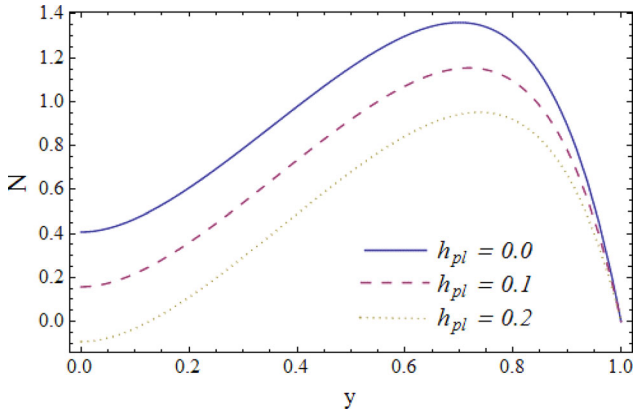

Figure 7. Impact of h_{pl} on micro-angular velocity field with $x = 1$, $\kappa = 1$, $m = 6$, $u_e = 1$, $w = 0.2$.

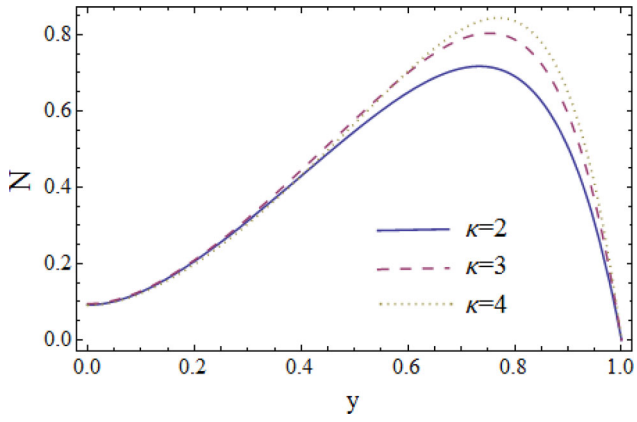

Figure 8. Impact of κ on micro-angular velocity field with $h_{pl} = 0.1$ $x = 1$, $m = 6$, $u_e = 1$, $w = 0.2$.

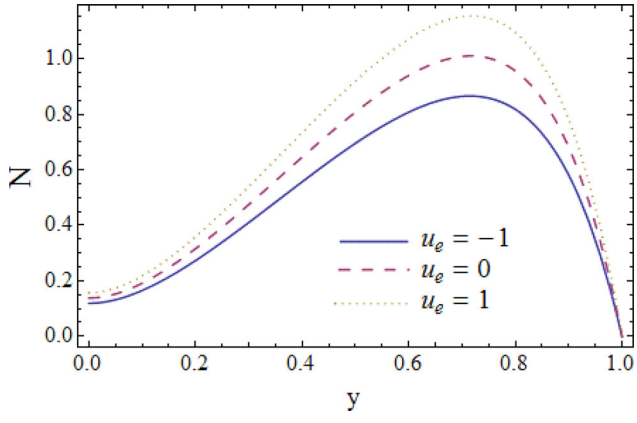

Figure 9. Impact of u_e on micro-angular velocity field with $h_{pl} = 0.1$ $x = 1$, $m = 6$, $\kappa = 1$, $w = 0.2$.

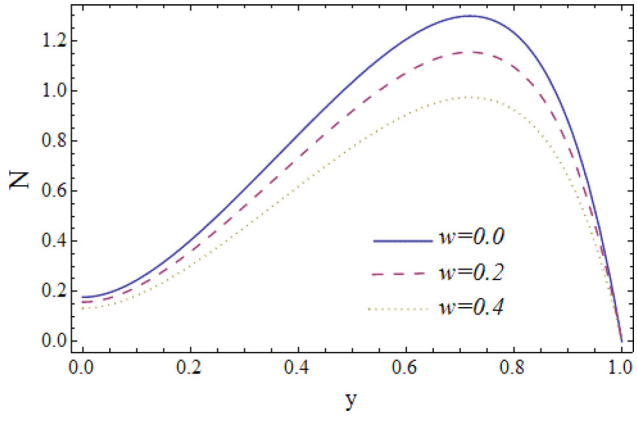

Figure 10. Impact of w on micro-angular velocity field with $h_{pl} = 0.1$ $x = 1$, $m = 6$, $\kappa = 1$, $u_e = 1$.

5. Conclusion

In the present analysis, a theoretical analysis is presented to study the electroosmotic flow of a micropolar Bingham viscoplastic fluid. Analytical solutions are obtained for axial and micro-angular velocity. The pumps that include combine benefits of both electroosmosis and peristalsis are widely used due to their applications. The highly applicable areas of electroosmosis phenomenon involves drug delivery by diagnostic medical apprautus, treatment of diseases, (i.e., sickle cell, anomaly in cells and blood related medical problems.). Further, main advantages of such electroosmotic pumps are their efficiency and low cost working. The obtained results are analyzed by plotting

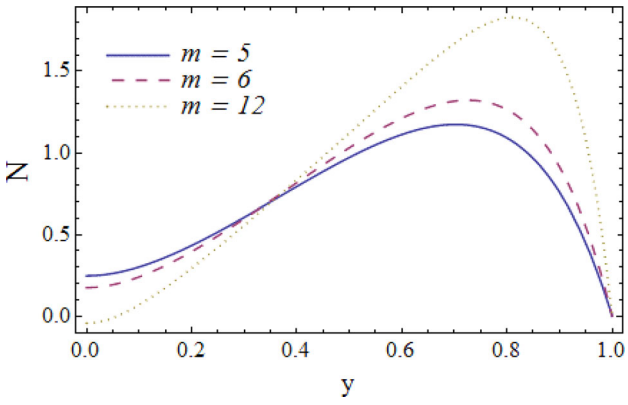

Figure 11. Impact of m on micro-angular velocity field with $h_{pl} = 0.1,\ x = 1,\ \kappa = 2,\ u_e = 1,\ w = 0.2$.

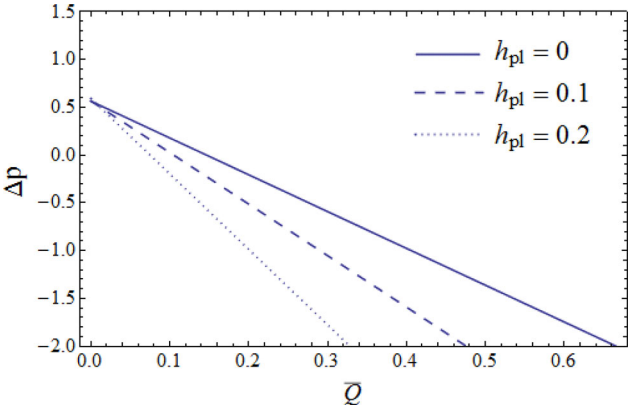

Figure 12. Impact of h_{pl} on pressure gradient with $x = 1,\ \kappa = 1,\ m = 6,\ u_e = 1,\ w = 0.2$.

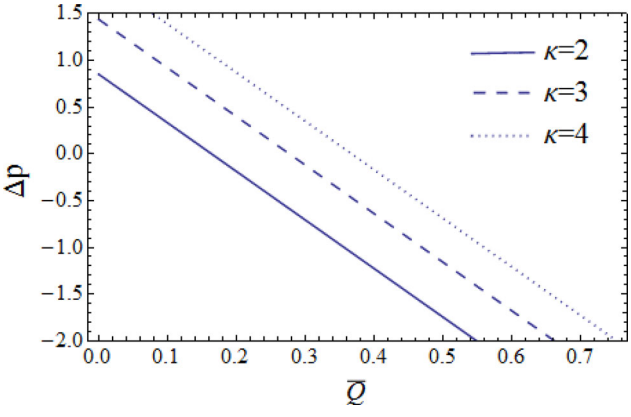

Figure 13. Impact of κ on pressure gradient with $x = 1, h_{pl} = 0.1,\ m = 6,\ u_e = 1,\ w = 0.2$.

graphical outcomes for various physical parameters that are included in this mathematical problem. The graphical results show the impact of various parameters that how these parameters are effecting the flow physically. The impact of Helmholtz-Smoluchowski velocity, Debye-length parameter, plug flow width, coupling number and micropolar parameter on axial velocity u, micro-angular velocity N pressure difference

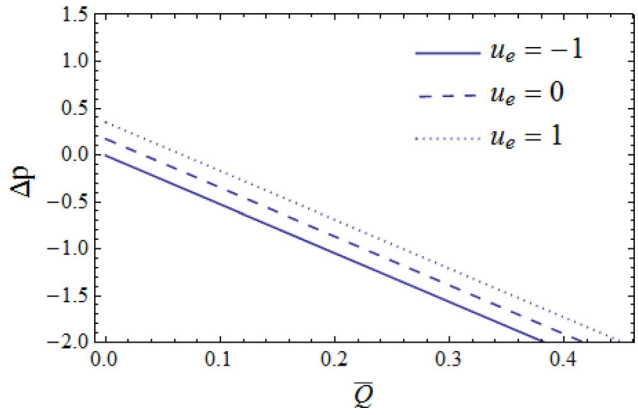

Figure 14. Impact of u_e on pressure gradient with $x = 1, h_{pl} = 0.1,\ m = 6,\ \kappa = 1,\ w = 0.2$.

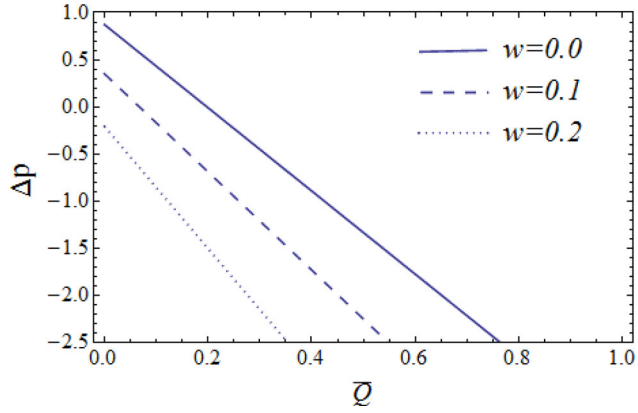

Figure 15. Impact of w on pressure gradient with $x = 1, h_{pl} = 0.1,\ m = 6,\ \kappa = 1,\ u_e = 1$.

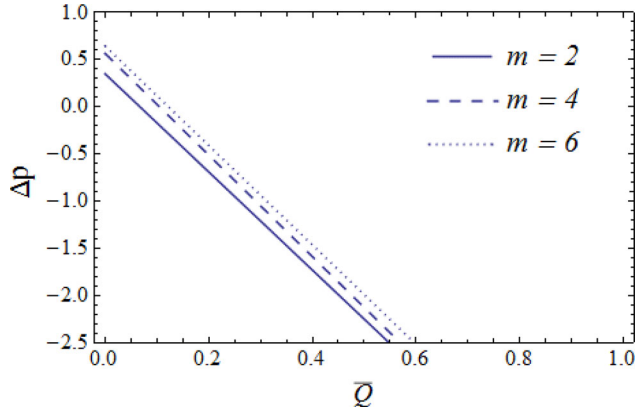

Figure 16. Impact of m on pressure gradient with $x = 1,\ h_{pl} = 0.1,\ w = 0.2,\ \kappa = 1,\ u_e = 1$.

Δp, and shear stress τ_{xy} is plotted by using Mathematica 9.0. From the current analysis, it is concluded that:

- Axial velovity u declines with the rise in plug flow width and coupling number whereas increases with Helmholtz-Smoluchowski velocity, Debye length parameter and micropolar parameter.

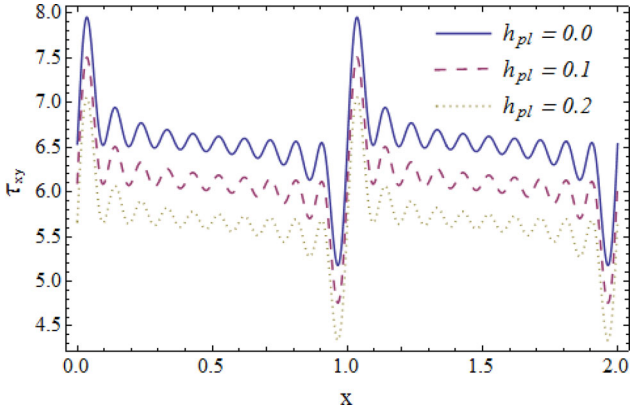

Figure 17. Impact of h_{pl} on wall shear stress with $\kappa = 1$, $m = 6$, $u_e = 1$, $w = 0.2$.

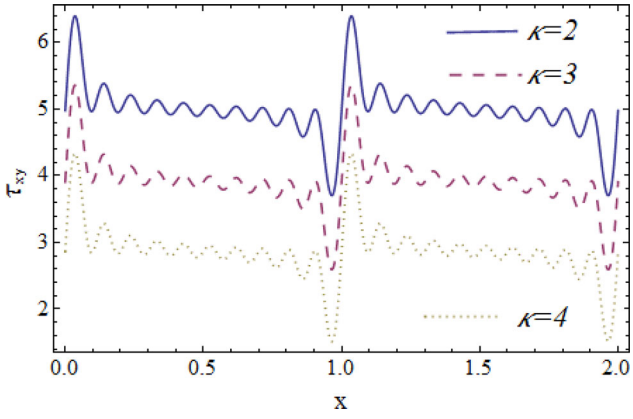

Figure 18. Impact of κ on wall shear stress with $h_{pl} = 0.1$, $m = 6$, $u_e = 1$, $w = 0.2$.

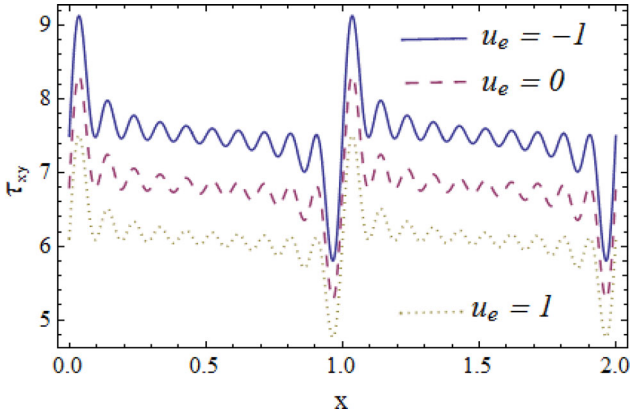

Figure 19. Impact of u_e on wall shear stress with $h_{pl} = 0.1$, $m = 6$, $\kappa = 1$, $w = 0.2$.

- Micro-angular velocity N increases with Helmholtz-Smoluchowski velocity, Debye length parameter and micropolar parameter however, there is opposite impact for plug flow width and coupling number.
- Pressure gradient decays with an increase in plug flow width and coupling number but increases with Helmholtz-Smoluchowski velocity, Debye length parameter, and micropolar parameter.
- Shear stress decreases with the growth in Debye length parameter, Helmholtz-Smoluchowski velocity as well as plug flow width. However, no change is detected in the case of the coupling number and micropolar parameter.

Disclosure statement

No potential conflict of interest was reported by the author(s).

References

Abbas SZ, Khan MI, Kadry S, Khan WA, Israr-Ur-Rehman M, Waqas M. 2020. Fully developed entropy optimized second order velocity slip MHD nanofluid flow with activation energy. Comput Methods Programs Biomed. 190: 105362.

Abbas SZ, Khan WA, Kadry S, Khan MI, Waqas M, Khan MI. 2020. Entropy optimized Darcy-Forchheimer nanofluid (silicon dioxide, molybdenum disulfide) subject to temperature dependent viscosity. Comput Methods Programs Biomed. 190:105363.

Abd Elmaboud Y, Abdelsalam SI, Mekheimer KS, Vafai K. 2019. Electromagnetic flow for two-layer immiscible fluids. Eng Sci Technol IntJ. 22(1):237–248.

Abdelsalam SI, Bhatti MM. 2018a. The impact of impinging TiO2 nanoparticles in Prandtl nanofluid along with endoscopic and variable magnetic field effects on peristaltic blood flow. Multi Modelg in Mat & Struct. 14(3): 530–548.

Abdelsalam SI, Bhatti MM. 2018b. The study of non-Newtonian nanofluid with hall and ion slip effects on peristaltically induced motion in a non-uniform channel. RSC Adv. 8(15):7904–7915.

Abdelsalam SI, Bhatti MM. 2019. New insight into AuNP applications in tumour treatment and cosmetics through wavy annuli at the nanoscale. Sci Rep. 9(1):1–14.

Abdelsalam SI, Bhatti MM. 2020. Anomalous reactivity of thermo-bioconvective nanofluid towards oxytactic microorganisms. Appl Math Mech-Engl Ed. 41(5):711–724.

Abdelsalam SI, Bhatti MM, Zeeshan A, Riaz A, Beg OA. 2019. Metachronal propulsion of electrically-conducting viscoelastic particle-fluid suspension in a ciliated channel under transverse magnetic field: mathematical modelling. Phys Scr. 94(11):115301–115314.

Abdelsalam SI, Mekheimer KS. 2018. Couple stress fluid flow in a rotating channel with peristalsis. J Hydrodyn. 30(2):307–316.

Abdelsalam SI, Sohail M. 2020. Numerical approach of variable thermophysical features of dissipated viscous nanofluid comprising gyrotactic micro-organisms. Pramana J Phys. 94(1):67.

Abdelsalam SI, Vafai K. 2017a. Combined effects of magnetic field and rheological properties on the peristaltic flow of a compressible fluid in a microfluidic channel. Eur J Mech B Fluids. 65:398–411.

Abdelsalam SI, Vafai K. 2017b. Particulate suspension effect on peristaltically induced unsteady pulsatile flow in a narrow artery: blood flow model. Math Biosci. 283: 91–105.

Abumandour RM, Eldesoky IM, Kamel MH, Ahmed MM, Abdelsalam SI. 2020. Peristaltic thrusting of a thermal-viscosity nanofluid through a resilient vertical pipe. Zeitschrift Für Naturforschung A. 75(8):727–738.

Arulanandam S, Li D. 2000. Liquid transport in rectangular microchannels by electro-osmotic pumping. Colloids Surf A. 161(1):89–102.

Dhinakaran S, Afonso AM, Alves MA, Pinho FT. 2010. Steady viscoelastic fluid flow between parallel plates under electroosmotic forces: Phan-Thien-Tanner model. J Colloid Interface Sci. 344(2):513–520.

Ding Z, Jian Y, Wang L, Yang L. 2017. Analytical investigation of electrokinetic effects of micropolar fluids in nanofluidic channels. Phys Fluids. 29(8):082008.

Ding Z, Jian Y, Yang L. 2016. Time periodic electroosmotic flow of micropolar fluids through microparallel channel. Appl Math Mech-Engl Ed. 37(6):769–786.

Eldesoky IM, Abdelsalam SI, El-Askary WA, Ahmed MM. 2019. Concurrent development of thermal energy with magnetic field on a particle-fluid suspension through a porous conduit. BioNanoSci. 9(1):186–202.

Eldesoky I, Abdelsalam S, El-Askary W, El-Refaey A, Ahmed M. 2019. Joint effect of thermal energy and magnetic field on particulate fluid suspension in a catheterized tube. BioNanoSci. 9(3):723–739.

Elkoumy SR, Barakat EI, Abdelsalam SI. 2013. Hall and transverse magnetic field effects on peristaltic flow of a Maxwell fluid through a porous medium. Global J Pure Appl Math. 9(2):187–203.

Haghighi AR, Aliashrafi N, Asl MS. 2020. An implicit approach to the micropolar fluid model of blood flow under the effect of body acceleration. Math Sci. 14(3): 269–277.

Haghighi AR, Asl MS. 2015. Mathematical modeling of micropolar fluid flow through an overlapping arterial stenosis. Int J Biomath. 08(04):1550056.

Haghighi AR, Asl MS, Kiyasatfar M. 2015. Mathematical modeling of unsteady blood flow through elastic tapered artery with overlapping stenosis. J Braz Soc Mech Sci Eng. 37(2):571–578.

Hayat T, Khan MI, Farooq M, Alsaedi A, Waqas M, Yasmeen T. 2016. Impact of Cattaneo–Christov heat flux model in flow of variable thermal conductivity fluid over a variable thicked surface. Int J Heat Mass Transf. 99: 702–710.

Ijaz Khan M, Alzahrani F. 2020. Activation energy and binary chemical reaction effect in nonlinear thermal radiative stagnation point flow of Walter-B nanofluid: Numerical computations. Int J Mod Phys B. 34(13): 2050132.

Jaffrin MY, Shapiro AH. 1971. Peristaltic pumping. Annu Rev Fluid Mech. 3(1):13–36.

Jiménez E, Escandón J, Bautista O, Méndez F. 2016. Start-up electroosmotic flow of Maxwell fluids in a rectangular microchannel with high zeta potentials. J Non-Newton Fluid Mech. 227:17–29.

Khan MI, Alsaedi A, Qayyum S, Hayat T, Khan MI. 2019. Entropy generation optimization in flow of Prandtl–Eyring nanofluid with binary chemical reaction and Arrhenius activation energy. Colloids Surf A. 570: 117–126.

Khan MI, Alzahrani F, Hobiny A. 2020a. Heat transport and nonlinear mixed convective nanomaterial slip flow of Walter-B fluid containing gyrotactic microorganisms. Alexandria Eng J. 59(3):1761–1769.

Khan MI, Alzahrani F, Hobiny A. 2020b. Simulation and modeling of second order velocity slip flow of micropolar ferrofluid with Darcy–Forchheimer porous medium. J Mater Res Technol. 9(4):7335–7340.

Khan MI, Qayyum S, Hayat T, Alsaedi A, Khan MI. 2018. Investigation of Sisko fluid through entropy generation. J Mol Liq. 257:155–163.

Khan MI, Qayyum S, Hayat T, Khan MI, Alsaedi A. 2019. Entropy optimization in flow of Williamson nanofluid in the presence of chemical reaction and Joule heating. Int J Heat Mass Transf. 133:959–967.

Khan MI, Qayyum S, Kadry S, Khan WA, Abbas SZ. 2020. Irreversibility analysis and heat transport in squeezing nanoliquid flow of non-Newtonian (second-grade) fluid between infinite plates with activation energy. Arab J Sci Eng. 45:4939–4947.

Khan MI, Waqas M, Hayat T, Alsaedi A. 2017. A comparative study of Casson fluid with homogeneous-heterogeneous reactions. J Colloid Interface Sci. 498:85–90.

Latham TW. 1966. Fluid motions in a peristaltic pump [M.S. thesis], MIT.

Lemoff AV, Lee AP. 2000. An AC magnetohydrodynamic micropump. Sens Actuators B. 63(3):178–185.

Maiti S, Misra JC. 2012. Peristaltic transport of a couple stress fluid: some applications to hemodynamics. J Mech Med Biol. 12(03):1250048.

Mekheimer KS, Abd Elmaboud Y. 2008. The influence of a micropolar fluid on peristaltic transport in an annulus: application of the clot model. Appl Bionics Biomech. 5(1):13–23.

Mekheimer KS, Komy SR, Abdelsalam SI. 2013. Simultaneous effects of magnetic field and space porosity on compressible Maxwell fluid transport induced by a surface acoustic wave in a microchannel. Chinese Phys B. 22(12):124702.

Misra JC, Ghosh SK. 2001. A mathematical model for the study of interstitial fluid movement vis-a-vis the non-Newtonian behaviour of blood in a constricted artery. Comput Math Appl. 41(5-6):783–811.

Misra JC, Pal B, Pal A, Gupta AS. 2001. Oscillatory entry flow in a plane channel with pulsating walls. Int J Non Linear Mech. 36(5):731–741.

Muhammad R, Khan MI, Khan NB, Jameel M. 2020. Magnetohydrodynamics (MHD) radiated nanomaterial viscous material flow by a curved surface with second order slip and entropy generation. Comput Methods Programs Biomed. 189:105294

Nadeem S, Kiani MN, Saleem A, Issakhov A. 2020. Microvascular blood flow with heat transfer in a wavy channel having electroosmotic effects. Electrophoresis. 41(13-14):1198–1205.

Nayak MK, Shaw S, Khan MI, Pandey VS, Nazeer M. 2020. Flow and thermal analysis on Darcy-Forchheimer flow of copper-water nanofluid due to a rotating disk: A static

and dynamic approach. J Mater Res Technol. 9(4): 7387–7408.
Ng CO. 2013. Combined pressure-driven and electroosmotic flow of Casson fluid through a slit microchannel. J Non-Newton Fluid Mech. 198:1–9.
Ng CO, Qi C. 2014. Electroosmotic flow of a power-law fluid in a non-uniform microchannel. J Non-Newton Fluid Mech. 208-209:118–125.
Pandey SK, Tripathi D. 2011. A mathematical model for peristaltic transport of micro-polar fluids. Appl Bionics Biomech. 8(3-4):279–293.
Pandey SK, Chaube MK. 2011. Peristaltic flow of a micropolar fluid through a porous medium in the presence of an external magnetic field. Commun Nonlinear Sci Numer Simul. 16(9):3591–3601.
Qayyum S, Khan MI, Hayat T, Alsaedi A. 2018. Comparative investigation of five nanoparticles in flow of viscous fluid with Joule heating and slip due to rotating disk. Physica B. 534:173–183.
Richter A, Plettner A, Hofmann KA, Sandmaier H. 1991. A micromachined electrohydrodynamic (EHD) pump. Sens Actuators A. 29(2):159–168.
Sadaf H, Abdelsalam SI. 2020. Adverse effects of a hybrid nanofluid in a wavy non-uniform annulus with convective boundary conditions. RSC Adv. 10(26):15035–15043.
Shapiro AH, Jaffrin MY, Weinberg SL. 1969. Peristaltic pumping with long wavelengths at low Reynolds number. J Fluid Mech. 37(4):799–825.
Shelukhin VV, Neverov VV. 2016. Thermodynamics of micropolar Bingham fluids. J Non-Newtonian Fluid Mech. 238:16–23.
Si D, Jian Y. 2015. Electromagnetohydrodynamic (EMHD) micropump of Jeffrey fluids through two parallel microchannels with corrugated walls. J Phys D: Appl Phys. 48(8):085501.
Sohail M, Naz R, Abdelsalam SI. 2020. Application of non-Fourier double diffusions theories to the boundary-layer flow of a yield stress exhibiting fluid model. Physica A. 537:122753.
Srivastava LM, Srivastava VP. 1984. Peristaltic transport of blood: casson model-II. J Biomech. 17(11):821–829.
Tripathi D, Yadav A, Bég OA, Kumar R. 2018. Study of microvascular non-Newtonian blood flow modulated by electroosmosis. Microvasc Res. 117:28–36.
van Lintel HTG, van de Pol FCM, Bouwstra S. 1988. A piezoelectric micro pump based on micromachining of silicon. Sens. Actuators. 15(2):153–167.
Wang J, Khan MI, Khan WA, Abbas SZ, Khan MI. 2020. Transportation of heat generation/absorption and radiative heat flux in homogeneous-heterogeneous catalytic reactions of non-Newtonian fluid (Oldroyd-B model). Comput Methods Programs Biomed. 189:105310
Wang J, Muhammad R, Khan MI, Khan WA, Abbas SZ. 2020. Entropy optimized MHD nanomaterial flow subject to variable thicked surface. Comput Methods Programs Biomed. 189:105311.